On Mode Conversion in Geometrically Unbalanced Differential Lines and Its Analogy With Crosstalk

Flavia Grassi, *Senior Member, IEEE*, Yuehong Yang, Xinglong Wu, Giordano Spadacini, *Member, IEEE*, and Sergio A. Pignari, *Fellow, IEEE*

I. Introduction

EFFECTIVE transmission of high-frequency signals is usually achieved by the use of differential lines, that is, two signal wires/traces operated according to a differential signaling scheme. The advantages in terms of electromagnetic compatibility (EMC) properties are several. Namely, a differential line does not theoretically radiate and is ideally immune to external interfering fields, since unwanted common mode (CM) disturbance cancels out at the line terminals [1]. However, in actual differential pairs, the imbalance possibly introduced by uncertainty and tolerances in the manufacturing process [2] as well as by nonideal behavior of circuit components may seriously degrade EMC performance due to undesired conversion of the differential mode (DM) into CM, and vice versa. Namely, DM-to-CM conversion is at the basis of unwanted radiated emissions (RE), whereas radiated susceptibility mainly originates from the conversion of the CM noise picked-up from external electromagnetic sources into DM disturbance at the ports of the drivers/receivers connected at the line ends.

Due to the relevance of this problem, unbalanced transmission lines (TLs) and mode conversion have been extensively studied both from the theoretical and experimental viewpoints [3]–[13]. Moreover, in order to quantify the amount of mode conversion, *ad hoc* parameters (such as the longitudinal and transverse conversion loss, foreseen by International Standards for telecommunication cables [14]), test setups [15], and measurement instruments [16] are currently exploited. Particularly, differential-line imbalance may arise due to line terminal sections [11]–[13], [17]–[19] or due to undesired asymmetries in the realization of the wiring structure, [6]–[10]. More precisely, asymmetries in the line cross section give rise to the so-called geometrical imbalance [5], [7], whereas the presence of wires/traces with different length is responsible for time imbalance [8]–[10].

In a previous work [11], imbalance due to the terminal networks was analyzed, and a circuit representation of mode conversion involving controlled sources was proposed, by recognizing the dominant DM and CM nature of signal transmission and field-to-wire coupling, respectively, and by introducing the concept of *weak imbalance.* Conversely, geometrical imbalance is considered in this paper, and the assumption of weak imbalance is rephrased to give a comprehensive circuit interpretation—by equivalent modal circuits—of the mode conversion due to asymmetries possibly affecting the differential-line cross section. The presented analysis will focus on DM-to-CM conversion only, but the proposed approach is general, and can be readily extended to the opposite conversion of CM into DM.

Novelty of the proposed approach stems from the interpretation of the conversion of the DM signal (dominant mode, driving the differential line) into undesired CM voltages and currents (second-order effect, responsible for RE) as the modal counterpart of crosstalk, where the generator circuit induces undesired voltages and currents into the receptor circuit, i.e., the circuit victim of interference [1], [20]. In crosstalk, the coupling between the generator and receptor circuit is due to the mutual inductance and capacitance between the two circuits. In a similar fashion, in mode conversion, the DM and CM circuits are coupled via inductive and capacitive imbalance coefficients proportional to the asymmetries exhibited by per unit length (p.u.l.) inductance and capacitance matrices associated with the line cross section. By virtue of this analogy, the assumption of weak coupling is rephrased in the modal domain in terms of weak imbalance, and the interference due to DM voltages/currents is modeled into the CM circuit by infinitesimal sources distributed along the line length. In order for such an inherently distributed nature of mode conversion to be correctly included into the prediction model, the TL equations of an infinitesimal CM line section are suitably reformulated, and solved in closed form to predict: 1) CM voltages and currents at the line terminal sections (quan-

Manuscript received June 26, 2014; revised September 24, 2014; accepted October 31, 2014. Date of publication December 8, 2014; date of current version April 13, 2015.

F. Grassi, G. Spadacini, and S. A. Pignari are with the Department of Electronics, Information and Bioengineering, Politecnico di Milano, Milan 20133, Italy (e-mail: flavia.grassi@polimi.it; giordano.spadacini@polimi.it; sergio.pignari@polimi.it).

Y. Yang and X. Wu are with the State Key Laboratory of Electrical Insulation and Power Equipment, Xi'an Jiaotong University, Xi'an 710049, China (e-mail: xjtuyyh@gmail.com; xjtuwuxinglong@gmail.com).

Color versions of one or more of the figures in this paper are available online.

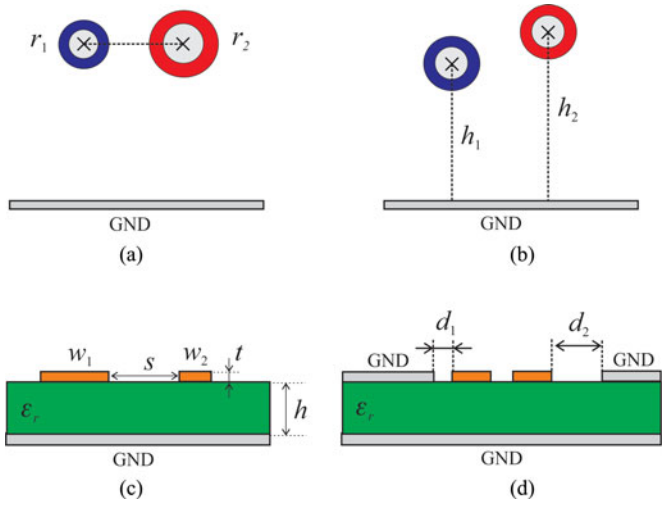

Fig. 1. Examples of line cross sections affected by geometrical imbalance.

tities strictly related to conversion loss parameters in [14]); and 2) the CM current distribution (key-ingredient for the prediction of near and far-field radiation from the differential line [1]).

This paper is organized as follows. In Section II, the wiring structure under analysis is described, and relevant parameters for the analysis are introduced. In Sections III and IV, an approximate CM circuit, in which effects due to geometrical imbalance are modeled by induced current and voltage sources, is derived and numerically validated. The analogy to crosstalk is made evident in Section V by the use of a suitable low-frequency (LF) model. The model is experimentally validated in Section VI, and concluding remarks are drawn in Section VII.

II. Wiring Structure Under Analysis

A. Differential Lines With Geometrical Imbalance

Practical examples of differential lines with cross sections affected by geometrical imbalance are sketched in Fig. 1. In these lines, geometrical imbalance originates from the presence of signal lines: 1) with different radius/width [as in Fig. 1(a) and (c)]; or 2) with different distance from the reference ground [as in Fig. 1(b) and (d)]. Apart from the specific structure under analysis, the corresponding p.u.l. inductance and capacitance matrices take the general expression:

$$\boldsymbol{L} = \begin{bmatrix} \ell_1 & \ell_m \\ \ell_m & \ell_2 \end{bmatrix}, \quad \boldsymbol{C} = \begin{bmatrix} c_1 & -c_m \\ -c_m & c_2 \end{bmatrix} \tag{1}$$

where inequality of diagonal entries, i.e., $\ell_1 \neq \ell_2$, $c_1 \neq c_2$, is at the basis of geometrical imbalance. Indeed, introduction of the similarity transformation matrices [4]

$$\boldsymbol{T}_V = \begin{bmatrix} 1 & 1/2 \\ 1 & -1/2 \end{bmatrix}, \quad \boldsymbol{T}_I = \begin{bmatrix} 1/2 & 1 \\ 1/2 & -1 \end{bmatrix} \tag{2}$$

to express line voltages and currents in terms of CM and DM quantities as

$$\begin{pmatrix} V_1 \\ V_2 \end{pmatrix} = \boldsymbol{T}_V \cdot \begin{pmatrix} V_{\mathrm{CM}} \\ V_{\mathrm{DM}} \end{pmatrix}, \quad \begin{pmatrix} I_1 \\ I_2 \end{pmatrix} = \boldsymbol{T}_I \cdot \begin{pmatrix} I_{\mathrm{CM}} \\ I_{\mathrm{DM}} \end{pmatrix} \tag{3}$$

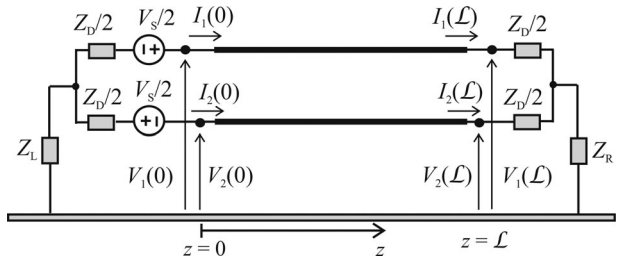

Fig. 2. Principle drawing of the differential line under analysis.

leads to the following expressions for the modal p.u.l. parameters matrices $\boldsymbol{L}_m = \boldsymbol{T}_V^{-1} \cdot \boldsymbol{L} \cdot \boldsymbol{T}_I$ and $\boldsymbol{C}_m = \boldsymbol{T}_I^{-1} \cdot \boldsymbol{C} \cdot \boldsymbol{T}_V$:

$$\boldsymbol{L}_m = \begin{bmatrix} \dfrac{\ell_1 + \ell_2 + 2\ell_m}{4} & \dfrac{\ell_1 - \ell_2}{2} \\ \dfrac{\ell_1 - \ell_2}{2} & \ell_1 + \ell_2 - 2\ell_m \end{bmatrix} = \begin{bmatrix} \ell_{\mathrm{CM}} & \Delta\ell \\ \Delta\ell & \ell_{\mathrm{DM}} \end{bmatrix} \tag{4}$$

$$\boldsymbol{C}_m = \begin{bmatrix} c_1 + c_2 - 2c_m & \dfrac{c_1 - c_2}{2} \\ \dfrac{c_1 - c_2}{2} & \dfrac{c_1 + c_2 + 2c_m}{4} \end{bmatrix} = \begin{bmatrix} c_{\mathrm{CM}} & \Delta c \\ \Delta c & c_{\mathrm{DM}} \end{bmatrix} \tag{5}$$

where out-diagonal entries $\Delta\ell$, Δc (ideally null in the case of well-balanced wiring structures) are responsible for distributed coupling (and mode conversion) between the DM and CM lines with p.u.l. parameters ℓ_{DM}, c_{DM} and ℓ_{CM}, c_{CM}, respectively. The degree of coupling between these modal lines depends on the amount of geometrical imbalance affecting the line cross section, and can be quantified (in analogy to crosstalk) by introducing inductive and capacitive imbalance coefficients as follows:

$$k_\ell = \frac{\Delta\ell}{\sqrt{\ell_{\mathrm{CM}}\ell_{\mathrm{DM}}}}, \quad k_c = \frac{\Delta c}{\sqrt{c_{\mathrm{CM}}c_{\mathrm{DM}}}}. \tag{6}$$

B. Line Terminal Sections

To analyze mode conversion due to geometrical imbalance, the differential line is modeled as a uniform and lossless multiconductor transmission line (MTL) terminated as in Fig. 2. The line is driven from the left end (i.e., $z = 0$) by two equal but opposite voltage sources $V_S/2$, assuring DM signaling.

Line terminal sections are assumed to be well-balanced, and modeled by lumped T-circuits with series impedances $Z_D/2$, and ground impedances Z_L, Z_R (for $Z_L = Z_R = 0\ \Omega$, this setup reproduces the impedance conditions for conversion-loss parameter measurement recommended in [14] and [15]). In terms of modal voltages and currents [see (2) and (3)], the port constraints at the terminations of the circuit in Fig. 2 can be cast as follows:

$$\begin{pmatrix} V_{\mathrm{CM}}(0) \\ V_{\mathrm{DM}}(0) \end{pmatrix} = \begin{pmatrix} 0 \\ V_S \end{pmatrix} - \begin{bmatrix} Z_L + Z_D/4 & 0 \\ 0 & Z_D \end{bmatrix} \cdot \begin{pmatrix} I_{\mathrm{CM}}(0) \\ I_{\mathrm{DM}}(0) \end{pmatrix} \tag{7}$$

$$\begin{pmatrix} V_{\mathrm{CM}}(\mathcal{L}) \\ V_{\mathrm{DM}}(\mathcal{L}) \end{pmatrix} = \begin{bmatrix} Z_R + Z_D/4 & 0 \\ 0 & Z_D \end{bmatrix} \cdot \begin{pmatrix} I_{\mathrm{CM}}(\mathcal{L}) \\ I_{\mathrm{DM}}(\mathcal{L}) \end{pmatrix}. \tag{8}$$

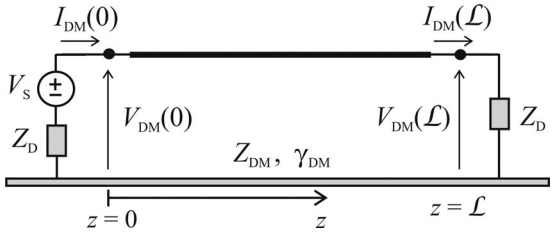

Fig. 3. Approximate DM equivalent circuit, obtained by neglecting the back interaction of CM currents/voltages on DM quantities.

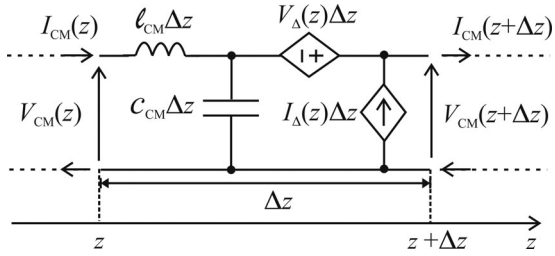

Fig. 4. Infinitesimal line section of the CM circuit: effects due to DM-to-CM conversion are modeled by infinitesimal voltage and current sources.

These expressions readily put in evidence the theoretical absence of any CM, which is neither excited by the DM source nor generated by imbalance of the terminal networks. Therefore, generation and propagation of CM currents, with detrimental consequences in terms of unwanted RE, can be ascribed to DM-to-CM conversion due to line imbalance only.

III. TL Equations

In the frequency domain, the first-order MTL equations of the wiring structure described in Section II can be written in the modal domain [see (2) and (3)] as

$$\frac{d}{dz}\boldsymbol{V}_m(z) = -j\omega\boldsymbol{L}_m \cdot \boldsymbol{I}_m(z) \tag{9}$$

$$\frac{d}{dz}\boldsymbol{I}_m(z) = -j\omega\boldsymbol{C}_m \cdot \boldsymbol{V}_m(z) \tag{10}$$

where $\boldsymbol{V}_m = \left(V_{\rm CM}\ V_{\rm DM}\right)^T$, $\boldsymbol{I}_m = \left(I_{\rm CM}\ I_{\rm DM}\right)^T$.

Due to the non-null entries $\Delta\ell,\ \Delta c$ in (4), (5), the system of equations in (9) and (10) is coupled and should be solved simultaneously for the unknown CM and DM voltages and currents by enforcing the port-constrains in (7) and (8).

However, as long as the DM and CM lines are weakly coupled, that is as long as geometrical imbalance is weak, the CM, which is not directly excited by the voltage source V_S, can be interpreted as a leakage of the dominant DM, and its back-interaction on DM quantities can be neglected. In analogy to crosstalk prediction [1], [20], the previous weak coupling condition can be rephrased in terms of the imbalance coefficients $k_\ell,\ k_c$ in (6) as: $\max\{k_\ell^2,\ k_c^2\} \ll 1$, that is, as a rule of thumb, $\max\{k_\ell^2,\ k_c^2\} < 0.1$.

From the standpoint of line solution, this means neglecting all contributions due to CM quantities in the equations related to the DM. Accordingly, DM-related equations in (9) and (10) can be approximated as follows:

$$\begin{aligned}\frac{dV_{\rm DM}(z)}{dz} &= -j\omega\left[\Delta\ell I_{\rm CM}(z) + \ell_{\rm DM} I_{\rm DM}(z)\right] \\ &\cong -j\omega\ell_{\rm DM} I_{\rm DM}(z) \end{aligned} \tag{11}$$

$$\begin{aligned}\frac{dI_{\rm DM}(z)}{dz} &= -j\omega\left[\Delta c V_{\rm CM}(z) + c_{\rm DM} V_{\rm DM}(z)\right] \\ &\cong -j\omega c_{\rm DM} V_{\rm DM}(z) \end{aligned} \tag{12}$$

and solved as the first-step, disregarding the presence of the CM circuit. Indeed, since line terminal sections are perfectly balanced, DM quantities can be readily predicted by solution of the equivalent modal TL in Fig. 3, where $\gamma_{\rm DM} = j\omega/v_{\rm DM}$, $v_{\rm DM} = \sqrt{\ell_{\rm DM} c_{\rm DM}}$, and $Z_{\rm DM} = \sqrt{\ell_{\rm DM}/c_{\rm DM}}$.

Once the DM circuit is solved and DM currents and voltages are known at each line position z, they behave as source terms for the CM equations, which can be accordingly rewritten in matrix form as

$$\frac{d}{dz}\begin{pmatrix} V_{\rm CM}(z) \\ I_{\rm CM}(z)\end{pmatrix} + j\omega\begin{bmatrix} 0 & \ell_{\rm CM} \\ c_{\rm CM} & 0\end{bmatrix}\cdot\begin{pmatrix} V_{\rm CM}(z) \\ I_{\rm CM}(z)\end{pmatrix} = \begin{pmatrix} V_\Delta(z) \\ I_\Delta(z)\end{pmatrix} \tag{13}$$

$$V_\Delta(z) = -j\omega\Delta\ell I_{\rm DM}(z) \tag{14}$$

$$I_\Delta(z) = -j\omega\Delta c V_{\rm DM}(z). \tag{15}$$

Equations (13)–(15) allow the circuit interpretation in Fig. 4, where an infinitesimal section of CM circuit is represented. According to this representation, DM-to-CM conversion is incorporated into the CM circuit by infinitesimal voltage and current sources, proportional to DM currents and voltages at line position z through the inductive and capacitive parameters $\Delta\ell$ and Δc, respectively.

IV. Equivalent CM Circuit

In this section, circuit interpretation and closed-form solution of the CM system of equations in (13)–(15) are addressed with the twofold objective of evaluating the CM quantities induced at line terminals (key-ingredients for estimating the conversion loss parameters in [14]) and the CM current distribution, from which REs can be predicted [1].

A. Prediction of CM Quantities at Line Terminals

By recognizing the direct analogy between the phasor form of TL equations in (13)—with spatial parameter z—and the equations of a lumped-parameter dynamic system—with time parameter t—the general solution of the system of equations in (13) can be cast as follows [21]:

$$\begin{pmatrix} V_{\rm CM}(z) \\ I_{\rm CM}(z)\end{pmatrix} = \boldsymbol{\Phi}(z)\cdot\begin{pmatrix} V_{\rm CM}(0) \\ I_{\rm CM}(0)\end{pmatrix} + \int_0^z \boldsymbol{\Phi}(z-\tau)\cdot\begin{pmatrix} V_\Delta(\tau) \\ I_\Delta(\tau)\end{pmatrix} d\tau \tag{16}$$

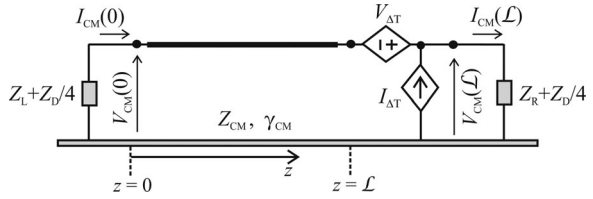

Fig. 5. Equivalent CM circuit at line terminals: effects due to DM-to-CM conversion are modeled by two lumped voltage and current sources connected at the right termination.

where

$$\mathbf{\Phi}(z) = \begin{bmatrix} \cosh(\gamma_{\rm CM} z) & -\sinh(\gamma_{\rm CM} z) Z_{\rm CM} \\ -\sinh(\gamma_{\rm CM} z) Z_{\rm CM}^{-1} & \cosh(\gamma_{\rm CM} z) \end{bmatrix} \quad (17)$$

and $\gamma_{\rm CM} = j\omega/v_{\rm CM}$, $v_{\rm CM} = \sqrt{\ell_{\rm CM} c_{\rm CM}}$, and $Z_{\rm CM} = \sqrt{\ell_{\rm CM}/c_{\rm CM}}$.

Starting from the general solution in (16), an equivalent CM circuit at line terminals can be obtained by evaluating (16) for $z = \mathcal{L}$. This yields

$$\begin{pmatrix} V_{\rm CM}(\mathcal{L}) \\ I_{\rm CM}(\mathcal{L}) \end{pmatrix} = \mathbf{\Phi}(\mathcal{L}) \cdot \begin{pmatrix} V_{\rm CM}(0) \\ I_{\rm CM}(0) \end{pmatrix} + \begin{pmatrix} V_{\Delta T} \\ I_{\Delta T} \end{pmatrix} \quad (18)$$

where the source vector

$$\begin{pmatrix} V_{\Delta T} \\ I_{\Delta T} \end{pmatrix} = \int_0^{\mathcal{L}} \mathbf{\Phi}(\mathcal{L}-\tau) \cdot \begin{pmatrix} -j\omega\Delta\ell I_{\rm DM}(\tau) \\ -j\omega\Delta c V_{\rm DM}(\tau) \end{pmatrix} d\tau \quad (19)$$

can be interpreted by a pair of lumped voltage and current sources connected at the right termination of the CM circuit as shown in Fig. 5.

Suitable analytical expressions for these sources can be obtained by expressing $I_{\rm DM}(\tau)$, $V_{\rm DM}(\tau)$ in (19) as function of the DM current at the right termination, i.e., $I_{\rm DM}(\mathcal{L})$. After some algebra, here omitted for brevity, $V_{\Delta T}$, $I_{\Delta T}$ take the closed-form expressions:

$$\frac{V_{\Delta T}}{I_{\rm DM}(\mathcal{L})} = j\omega\big[K_+(Sh_+ + \alpha Ch_+) - K_-(Sh_- + \alpha Ch_-) - \alpha(K_+ - K_-)\big] \quad (20)$$

$$\frac{I_{\Delta T}}{I_{\rm DM}(\mathcal{L})} = \frac{-j\omega}{Z_{\rm CM}}\big[K_+(Ch_+ + \alpha Sh_+) + K_-(Ch_- + \alpha Sh_-) - (K_+ + K_-)\big] \quad (21)$$

where $\alpha = Z_D/Z_{\rm DM}$ denotes the degree of mismatching of the DM circuit, and

$$Sh_\pm = \sinh\left[(\gamma_{\rm DM} \pm \gamma_{\rm CM})\mathcal{L}\right] \quad (22)$$

$$Ch_\pm = \cosh\left[(\gamma_{\rm DM} \pm \gamma_{\rm CM})\mathcal{L}\right] \quad (23)$$

$$K_\pm = \frac{\Delta c Z_{\rm CM} Z_{\rm DM} \mp \Delta\ell}{2(\gamma_{\rm DM} \pm \gamma_{\rm CM})}. \quad (24)$$

B. Prediction of the CM Current Distribution

In addition to voltages and currents at line terminals, the model in (16) and (17) allows evaluating the CM current distribution at each line position z, as key-ingredient to predict the RE generated by the differential line in the presence of geometrical imbalance.

Indeed, starting from (16), the CM current at line position z can be written as the sum of two contributions as $I_{\rm CM}(z) = I'_{\rm CM}(z) + I''_{\rm CM}(z)$. The first contribution, i.e.,

$$I'_{\rm CM}(z) = -\sinh(\gamma_{\rm CM} z) Z_{\rm CM}^{-1} V_{\rm CM}(0) + \cosh(\gamma_{\rm CM} z) I_{\rm CM}(0) \quad (25)$$

can be interpreted as the CM current distribution due to the lumped sources $V_{\Delta T}$, $I_{\Delta T}$ in (20) and (21), and can be easily evaluated by solution of the equivalent circuit in Fig. 5. This yields the expression:

$$I'_{\rm CM}(z) = \frac{\left[\beta_L \sinh(\gamma_{\rm CM} z) + \cosh(\gamma_{\rm CM} z)\right](Z_{\rm CM}^{-1} V_{\Delta T} - \beta_R I_{\Delta T})}{(\beta_L + \beta_R)\cosh(\gamma_{\rm CM}\mathcal{L}) + (1 + \beta_L\beta_R)\sinh(\gamma_{\rm CM}\mathcal{L})} \quad (26)$$

where $\beta_L = (Z_L + Z_D/4)/Z_{\rm CM}$ and $\beta_R = (Z_R + Z_D/4)/Z_{\rm CM}$ denote the degree of matching/mismatching of the CM circuit.

Conversely, the second contribution, i.e.,

$$I''_{CM}(z) = \int_0^z \mathbf{\Phi}(z-\tau) \cdot \begin{pmatrix} V_\Delta(\tau) \\ I_\Delta(\tau) \end{pmatrix} d\tau \quad (27)$$

is due to the infinitesimal voltage and current sources $V_\Delta(z)$, $I_\Delta(z)$ distributed along the CM TL, and cannot be predicted by the model in Fig. 5, which assures equivalence at line terminals only. Hence, explicit solution of the convolution integral in (27) is required, which yields

$$I''_{\rm CM}(z) = \frac{-j\omega I_{\rm DM}(\mathcal{L})}{Z_{CM}}\big[K_+(Ch'_+ + \alpha Sh'_+) + K_-(Ch'_- + \alpha Sh'_-) - (K_+ + K_-)(Ch_D + \alpha Sh_D)\big] \quad (28)$$

where K_+, K_- take the same expressions in (24), whereas $Sh'_\pm = \sinh(\gamma_{\rm DM}\mathcal{L} \pm \gamma_{\rm CM} z)$, $Ch'_\pm = \cosh(\gamma_{\rm DM}\mathcal{L} \pm \gamma_{\rm CM} z)$, $Sh_D = \sinh[\gamma_{\rm DM}(\mathcal{L} - z)]$, $Ch_D = \cosh[\gamma_{\rm DM}(\mathcal{L} - z)]$.

C. Validation Versus Exact Solution of MTL Equations

In this section, rigorous (exact) solution of MTL equations is used as reference to assess the accuracy of the predictions obtained by the approximate model here proposed, which neglects the back-interaction of CM quantities on the DM. To this end, different realizations of the PCB cross section sketched in Fig. 1(c) are considered. They are composed of a pair of coplanar microstrips printed on top of a double-face printed circuit board (PCB) with substrate height $h = 1.425$ mm, substrate relative permittivity $\varepsilon_r = 4.4$, and trace thickness $t = 35$ μm. The traces are kept at fix distance (i.e., $s = 0.5$ mm), but their width is varied so to test model accuracy for different degrees of imbalance. Particularly, the results shown in the following were obtained for the four test cases in Table I. Among these, the first cross section (i.e., PCB 1) was considered as the reference, since not affected by line imbalance, while the other ones were obtained starting from it by symmetrically increasing/decreasing

TABLE I
TRACE WIDTHS FOR THE PCBS UNDER ANALYSIS

	w_1	w_2
PCB 1	0.6 mm	0.6 mm
PCB 2	0.5 mm	0.7 mm
PCB 3	0.4 mm	0.8 mm
PCB 4	0.3 mm	0.9 mm

TABLE II
MODAL CHARACTERISTIC PARAMETERS FOR THE PCBS IN TABLE I

	PCB 1	PCB 2	PCB 3	PCB 4
$Z_{\rm DM}$ [Ω]	125.8	126.8	127.8	131
$Z_{\rm CM}$ [Ω]	65.2	65.4	65.6	66.4
$v_{\rm DM}$ [m/s]	1.85 10^8	1.85 10^8	1.83 10^8	1.82 10^8
$v_{\rm CM}$ [m/s]	1.69 10^8	1.69 10^8	1.68 10^8	1.66 10^8
k_ℓ	0	0.05	0.11	0.16
k_c	0	-0.06	-0.12	-0.19

the trace width w_1, w_2. The corresponding modal characteristic impedances, propagation velocities, and imbalance coefficients k_ℓ, k_c were evaluated by postprocessing according to (4) and (5) the p.u.l. parameters obtained by electrostatic simulation carried out by the FEM-based numerical code Maxwell [22]. The obtained values are listed in Table II, and show that, despite k_ℓ, k_c significantly increase from one realization to the other, the corresponding DM and CM characteristic impedances and propagation velocities are almost unchanged. In particular, since the DM characteristic impedance of all PCBs is around 125–130 Ω, for numerical simulation the series impedances of each terminal network were set to the value $Z_D = 100\ \Omega$, which leads to a mismatching coefficient for the DM circuit on the order of $\alpha \approx 0.76 - 0.8$. Predictions obtained by the approximate model here proposed (dashed curves) are compared versus those obtained by exact solution of MTL equations (solid curves) in Figs. 6 and 7, for two different values of the ground impedances Z_L, Z_R, that is, $Z_L = Z_R = 0\ \Omega$, and $Z_L = Z_R = 1$ kΩ, respectively. Simulations were carried out in the frequency interval from 1 MHz up to 2 GHz with a line length of 10 cm. The plots in (a) and (b) show the comparison in terms of DM (a) and CM (b) voltages at the right termination of the differential line (DM voltages have been plotted in a limited frequency range to improve figure readability). The comparison in terms of CM current distribution along the line length (at 1.5 GHz) is shown in (c). The comparison shows that, as long as the weak-imbalance assumption is satisfied, predictions obtained by the proposed model result to be in satisfactory agreement with those obtained by exact solution of MTL equations. In particular, even in the worst case here consider of a trace three times wider than the other (test case anyway satisfying the weak-imbalance condition in Section III, i.e., $k_c^2 \cong 0.036 \ll 1$), the maximum discrepancies are on the order of 0.1 dB for the DM, and of 1 dB for the CM. Conversely, for a degree of imbalance close to or exceeding the validity limit of the proposed model (i.e., $k_c^2 \cong 0.1$), prediction accuracy degrades both for the DM and the CM due to a gradually increasing shift of the resonance frequencies.

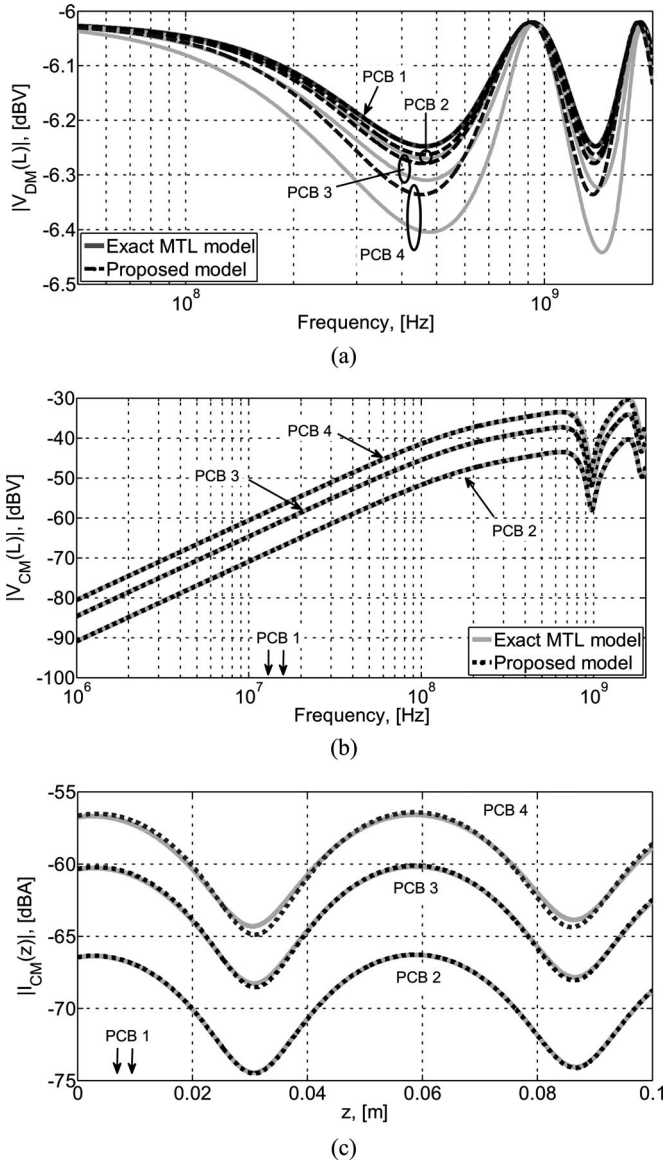

Fig. 6. Model validation versus exact solution of MTL equations (ground impedances: $Z_L = Z_R = 0\ \Omega$): (a) DM and (b) CM voltages at the right termination and (c) CM current distribution at 1.5 GHz.

V. LF MODEL AND ANALOGY WITH CROSSTALK

For electrically short TLs, LF expressions for the induced sources $V_{\Delta T}$, $I_{\Delta T}$ in (20) and (21) can be readily obtained by approximating the terms in (22) and (23) as follows: $Sh_\pm \cong (\gamma_{\rm DM} \pm \gamma_{\rm CM})\mathcal{L}, Ch_\pm \cong 1$. After some simple algebra, and by recognizing that $\alpha Z_{\rm DM} I_{\rm DM}(\mathcal{L}) = V_{\rm DM}(\mathcal{L})$, the following expressions are obtained:

$$V_{\Delta T} \cong -j\omega\Delta\ell\mathcal{L} I_{\rm DM}(\mathcal{L}) \tag{29}$$

$$I_{\Delta T} \cong -j\omega\Delta c\mathcal{L} V_{\rm DM}(\mathcal{L}). \tag{30}$$

These expressions exhibit a strict analogy to those involved in crosstalk analysis [1], [20], and have the potential to outline

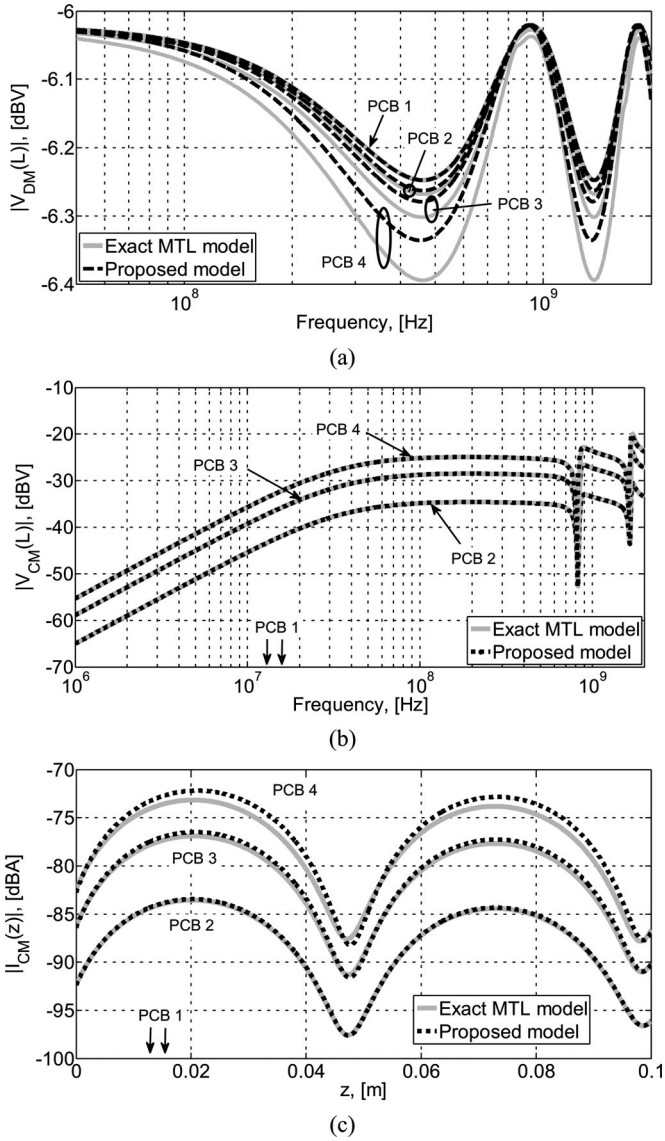

Fig. 7. Model validation versus exact solution of MTL equations (ground impedances: $Z_L = Z_R = 1$ kΩ): (a) DM and (b) CM voltages at the right termination and (c) CM current distribution at 1.5 GHz.

the twofold nature of mode conversion. Indeed, in [1] and [20], the LF model of the receptor circuit incorporates the interference due to the generator circuit by: 1) a voltage source proportional to the current into the generator circuit and to the total mutual inductance $L_m = \ell_m \mathcal{L}$ (inductive coupling) between the two circuits; and 2) a current source proportional to the voltage across the generator circuit and to the total mutual capacitance $C_m = c_m \mathcal{L}$ (capacitive coupling) between the two circuits. In a similar fashion, the interference due to the DM circuit (i.e., the modal circuit directly driven by the voltage source V_S) is included into the CM circuit by: 1) a voltage source $V_{\Delta T}$ proportional to the current in the DM circuit through the total inductance $\Delta L = \Delta\ell\mathcal{L}$; and 2) a current source $I_{\Delta T}$ proportional to the DM voltage through the total capacitance $\Delta C = \Delta c\mathcal{L}$. Additionally, currents and voltages in the *source* circuit (here, the DM circuit) can be computed by neglecting the presence of the *receptor* circuit (here, the CM circuit).

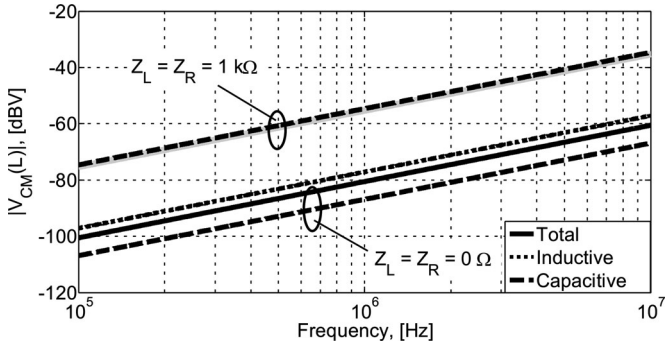

Fig. 8. LF model: inductive (dotted) and capacitive (dashed) contributions to the total (solid) CM voltage in (32) for two different values of $Z_L = Z_R$, that is: (a) $Z_L = Z_R = 0\ \Omega$ (lower curves) and (b) $Z_L = Z_R = 1$ kΩ (upper curves).

Likewise for crosstalk, at LF voltages and currents induced into the CM circuit increase with a frequency-slope of $+20$ dB/decade. Additionally, the predominance of one contribution over the other is strictly related to the value of the terminal loads. Indeed, the voltages (and currents) induced across the left (superscript *L*) and right (superscript *R*) terminations of the CM circuit can be written as the superposition of inductive and capacitive contributions (first and second terms into brackets, respectively) as follows:

$$V_{\rm CM}^{L} = -\frac{j\omega}{2}\left(-\frac{\Delta L}{\alpha Z_{\rm DM}} + \Delta C Z_{\rm CM}\beta_R\right)\frac{\beta_L}{\beta_L+\beta_R}V_S \quad (31)$$

$$V_{\rm CM}^{R} = -\frac{j\omega}{2}\left(\frac{\Delta L}{\alpha Z_{\rm DM}} + \Delta C Z_{\rm CM}\beta_L\right)\frac{\beta_R}{\beta_L+\beta_R}V_S. \quad (32)$$

Since in practically relevant cases the terminations of the DM circuit are designed to be almost matched to the DM characteristic impedance of the differential line (i.e., $\alpha \cong 1$), it can be concluded that the prevalence of one contribution over the other is mainly determined by the value of Z_L and Z_R. Indeed, the capacitive contribution is predominant for large values of Z_L and Z_R. Vice versa, if these impedances take small values, the inductive contribution is prevailing. Furthermore, starting from the results obtained for crosstalk, one would expect a partial compensation of inductive and capacitive contributions at the right termination (i.e., far from the source), and vice versa maximum interference at the left termination. The expressions in (31) and (32) apparently clash with this expectation, as the two contributions sum in (31) and subtract in (32). However, the contradiction is only apparent, since $\Delta\ell$ and Δc are always opposite in sign. Indeed, if the self-inductance of a signal line increases, its self-capacitance decreases, and vice versa (see Table II). As an explicative example, inductive (dotted curves) and capacitive (dashed curves) contributions to the total (solid curves) CM voltage $V_{\rm CM}^{R}$ in (32) are plotted in Fig. 8 for the last microstrip line in Section IV-C (see PCB 4 in Table I). Simulations were carried out from 100 kHz up to 10 MHz, and were obtained for two different values of ground impedances, that is $Z_L = Z_R = 0\ \Omega$ and $Z_L = Z_R = 1$ kΩ.

Since in both cases $Z_D = 100\ \Omega$, the inductive contribution (dotted curve) is the same, whereas the capacitive contribution increases proportionally to $Z_L = Z_R$. Therefore, while for

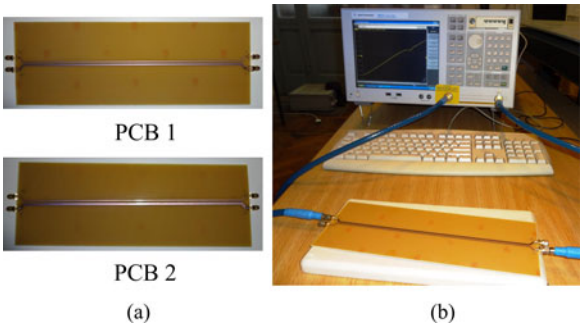

Fig. 9. (a) PCB boards and (b) measurement setup used for experimental validation of the proposed model.

TABLE III
MODAL PARAMETERS FOR THE PCBS IN FIG. 9(a)

	PCB 1	PCB 2
Z_{DM}	125 Ω	113 Ω
Z_{CM}	40 Ω	35.5 Ω
v_{DM}	1.78 10^8 m/s	1.72 10^8 m/s
v_{CM}	1.63 10^8 m/s	1.58 10^8 m/s
k_ℓ	0.14	0.24
k_c	−0.165	−0.28

$Z_L = Z_R = 0\ \Omega$ the inductive contribution is fairly larger than the capacitive one (actually, they are anyway comparable in magnitude, as a slight compensation between them is observed in the total voltage V^R_{CM}), for $Z_L = Z_R = 1\ \mathrm{k}\Omega$ DM-to-CM conversion can be fully ascribed to the capacitive contribution.

VI. EXPERIMENTAL VALIDATION

In this section, the prediction model in Section IV is validated versus the measurement data obtained by experimental characterization of the pairs of coplanar microstrips shown in Fig. 9(a). In both samples, the two traces are printed on top of a double-face PCB as in Fig. 1(c). Geometrical and material characteristics of the PCB boards are: substrate height $h = 1.6$ mm, substrate relative permittivity $\varepsilon_r = 4.4$, trace thickness $t = 35\ \mu$m, and trace length $\mathcal{L} = 280$ mm. The two traces are kept at distance $s = 2$ mm. However, they are affected by different degrees of imbalance. Namely, in both pairs, one trace has width $w_1 = 1$ mm, while the other one is made two times [i.e., $w_2 = 2$ mm in PCB1, Fig. 9(a)] and three times [i.e., $w_2 = 3$ mm in PCB2, Fig. 9(a)] wider. For these cross sections, numerical simulations [22] yield the modal characteristic impedances, propagation velocities, and imbalance coefficients in Table III, and show that, though with different margin, both PCBs satisfy the weak-imbalance condition: $\max\{k_\ell^2,\ k_c^2\} \ll 1$. Namely: $k_c^2 \cong 0.03$ for PCB 1, and $k_c^2 \cong 0.08$ for PCB 2. For the sake of comparison with the predictions obtained by the proposed model, the two PCBs were experimentally characterized at the four output ports in the frequency interval from 100 kHz up to 2 GHz. Measurements were carried out by a two-port vector network analyzer (VNA) Agilent ENA E5071C, by connecting the VNA ports in turn with a pair of SMA (Subminiature version A) ports of the PCB under

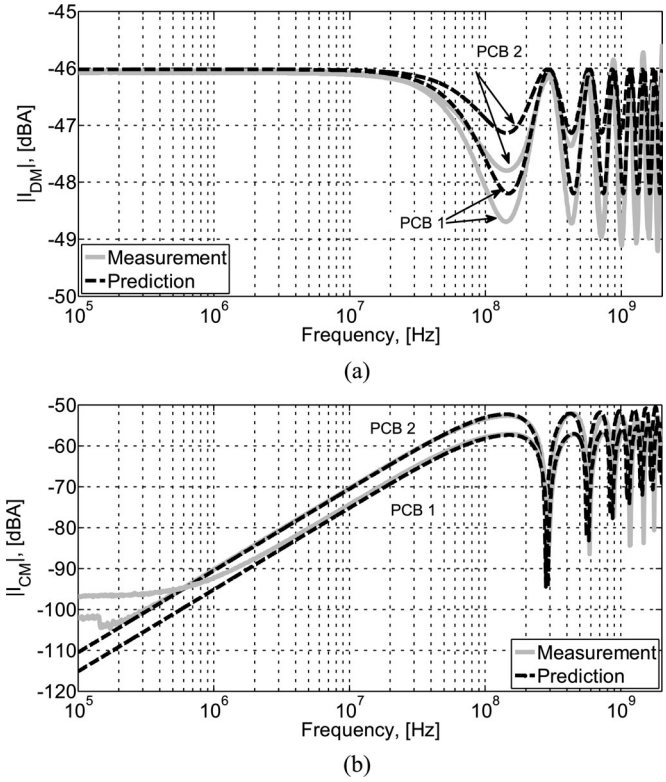

Fig. 10. (a) DM and (b) CM currents at the left termination of the PCBs in Fig. 9(a). Measurement (solid curves) versus prediction (dashed curves) obtained by the proposed model.

analysis, while the other two SMA ports were loaded by 50 Ω terminations [see Fig. 9(b)]. The obtained 4×4 scattering parameter matrices were then converted into chain-parameter notation, and used to evaluate DM and CM quantities at the terminations of each board. This led to the solid curves in Fig. 10, which represent (as a specific example) the DM (a) and CM (b) currents at the left termination for DM and CM impedances of the terminal networks equal to 100 and 25 Ω, respectively. (These values mimic the impedances adopted in typical setups for conversion loss measurement [14]–[16].) The corresponding predictions obtained by the proposed model are plotted in the same figure by dashed lines. For prediction, the overall line length was set equal to 300 mm, so to account for the presence of the two SMA connectors (10 mm long) soldered at the terminations of each PCB trace.

Even if the prediction model does not account for losses that are responsible for the attenuation experienced by the frequency response of the measured quantities above 1 GHz, the comparison shows a good agreement (this was also assessed by the feature selective validation technique [23]–[25]). This is true also for the CM current of PCB 2, which exhibits negligible shifts of the resonance frequencies (null-points), even if the degree of imbalance ($k_c^2 \cong 0.08$) is very close to the limit of validity of the proposed model.

VII. CONCLUSION

Under the assumption of *weak imbalance,* the strict analogy between crosstalk and DM-to-CM conversion occurring in

geometrically unbalanced differential lines has been unveiled, and a circuit interpretation of the phenomenon, allowing for accurate prediction of the undesired CM currents responsible for RE, has been proposed. With respect to exact solution of MTL equations, the proposed reformulation of the problem can represent a more powerful resource for the designer. As a matter of fact, since geometrical imbalance is usually to be ascribed to uncertainty and tolerances in the manufacture process, a statistical approach [2] is definitely more suited than a deterministic one to provide quantitative estimations of the involved CM quantities and consequent RE. In this respect, it is worth noting that—as long as the weak-imbalance assumption is satisfied—the proposed model has the advantage to treat the unbalanced differential line as a perturbation of the corresponding ideally balanced structure. Namely, it was proved that CM and DM characteristic impedances and propagation constants (see Table II) as well as DM predictions do not exhibit significant variations in the presence and absence of imbalance. Therefore, this perturbational approach enables sensitivity analyses of the involved CM quantities through repeated-run simulations or by stochastic models at the cost of limited computational burden [26].

Although conveniently derived for an ideal differential line in order to highlight general properties of mode conversion, the proposed model can be further extended to include nonideal effects in PCB traces, such as losses and dispersion, and additional phenomena of mode conversion, such as imbalance due to the terminal networks [11], and crosstalk coupling with nearby differential lines. Particularly, the inclusion of losses can be easily handled by accounting for complex-valued p.u.l. impedance and admittance matrices in (9) and (10). Additionally, crosstalk with nearby pairs can be addressed by reformulating the MTL equations and the weak imbalance assumption for the multipair structure under analysis.

REFERENCES

[1] C. R. Paul, *Introduction to Electromagnetic Compatibility*, 2nd ed. New York, NY, USA: Wiley, 2006.

[2] I. S. Stievano, P. Manfredi, and F. G. Canavero, "Stochastic analysis of multiconductor cables and interconnects," *IEEE Trans. Electromagn. Compat.*, vol. 53, no. 2, pp. 501–507, May 2011.

[3] V. K. Tripathi, "Asymmetric coupled transmission lines in an inhomogeneous medium," *IEEE Trans. Microw. Theory Tech.*, vol. MTT-23, no. 9, pp. 734–739, Sep. 1975.

[4] D. E. Bockelman and W. R. Eisenstadt, "Combined differential and common-mode scattering parameters: Theory and simulation," *IEEE Trans. Microw. Theory Tech.*, vol. 43, no. 7, pp. 1530–1539, Jul. 1995.

[5] S. B. Smith, S. S. Agili, and V. Balasubramanian, "Theory and measurement of unbalanced differential-mode transmission lines," presented at the DesignCon Conference, Santa Clara, CA, USA, Feb. 2006.

[6] C. Su and T. Hubing, "Imbalance difference model for common-mode radiation from printed circuit boards," *IEEE Trans. Electromagn. Compat.*, vol. 53, no. 1, pp. 150–156, Feb. 2011.

[7] K. Sejima, Y. Toyota, K. Iokibe, L. R. Koga, and T. Watanabe, "Experimental model validation of mode-conversion sources introduced to modal equivalent circuit," in *Proc. IEEE Int. Symp. Electromagn. Compat.*, Pittsburgh, PA, USA, Aug. 2012, pp. 492–497.

[8] Y. Kayano, Y. Tsuda, and H. Inoue, "Identifying EM radiation from asymmetrical differential-paired lines with equi-distance routing," in *Proc. IEEE Int. Symp. Electromagn. Compat.*, Pittsburgh, PA, USA, Aug. 2012, pp. 311–316.

[9] Y. Kayano, K. Mimura, and H. Inoue, "Evaluation of imbalance component and EM radiation generated by an asymmetrical differential-paired lines structure," *Trans. JIEP*, vol. 4, no. 1, pp. 6–16, Dec. 2011.

[10] G. H. Shiue, J. H. Shiu, Y. C. Tsai, and C. M. Hsu, "Analysis of common-mode noise for weakly coupled differential serpentine delay microstrip line in high-speed digital circuits," *IEEE Trans. Electromagn. Compat.*, vol. 54, no. 3, pp. 655–666, Jun. 2012.

[11] F. Grassi, G. Spadacini, and S. A. Pignari, "The concept of weak imbalance and its role in the emissions and immunity of differential lines," *IEEE Trans. Electromagn. Compat.*, vol. 55, no. 6, pp. 1346–1349, Dec. 2013.

[12] A. Sugiura and Y. Kami, "Generation and propagation of common-mode currents in a balanced two-conductor line," *IEEE Trans. Electromagn. Compat.*, vol. 54, no. 2, pp. 466–473, Apr. 2012.

[13] Y. Kami, F. Xiao, and K. Murano, "Mode-port-network approach to analyze power-line EMC problems for PLC," in *Proc. 20th Int. Zurich Symp. Electromagn. Compat.*, Zurich, Switzerland, Jun. 2009, pp. 9–12.

[14] *Transmission Aspects of Unbalance About Earth*, ITU-T Recommendation G.117, Geneva, Switzerland, 1989.

[15] I. P. Macfarlane, "A probe for the measurement of electrical unbalance of networks and devices," *IEEE Trans. Electromagn. Compat.*, vol. 41, no. 1, pp. 3–14, Feb. 1999.

[16] *Measuring Balanced Components With Vector Network Analyzer ZVB*, Rohde & Schwarz, Application Note 1EZ53, Sep. 2004.

[17] F. Grassi and S. A. Pignari, "Immunity to conducted noise of data transmission along DC power lines involving twisted-wire pairs above ground," *IEEE Trans. Electromagn. Compat.*, vol. 55, no. 1, pp. 195–207, Feb. 2013.

[18] F. Grassi and S. A. Pignari, "Bulk current injection in twisted-wire pairs with not perfectly balanced terminations," *IEEE Trans. Electromagn. Compat.*, vol. 55, no. 6, pp. 1293–1301, Dec. 2013.

[19] F. Grassi, G. Spadacini, and S. A. Pignari, "SPICE behavioral modeling of RF current injection in wire bundles," *IEICE Trans. Commun.*, vol. E97-B, no. 2, pp. 424–431, Feb. 2014.

[20] C. R. Paul, "On the superposition of inductive and capacitive coupling in crosstalk prediction models," *IEEE Trans. Electromagn. Compat.*, vol. EMC-24, no. 3, pp. 335–343, Aug. 1982.

[21] C. R. Paul, *Analysis of Multiconductor Transmission Lines*. New York, NY, USA: Wiley Interscience, 1994.

[22] Maxwell 3D v.10, Ansoft Corporation, 1984–2004.

[23] *Standard for Validation of Computational Electromagnetics Computer Modeling and Simulation—Part 1*, IEEE Standard P1597, Feb. 2008.

[24] A. P. Duffy, A. J. M. Martin, A. Orlandi, G. Antonini, T. M. Benson, and M. S. Woolfson, "Feature selective validation (FSV) for validation of computational electromagnetics (CEM). Part I–The FSV method," *IEEE Trans. Electromagn. Compat.*, vol. 48, no. 3, pp. 449–459, Aug. 2006.

[25] A. Orlandi, A. P. Duffy, B. Archambeault, G. Antonini, D. E. Coleby, and S. Connor, "Feature selective validation (FSV) for validation of computational electromagnetics (CEM). Part II—Assessment of FSV performance," *IEEE Trans. Electromagn. Compat.*, vol. 48, no. 3, pp. 460–467, Aug. 2006.

[26] X. Wu, Y. Yang, F. Grassi, G. Spadacini, and S. A. Pignari, "Statistical characterization of line-imbalance in differential lines," presented at the XXXIth General Assembly of International Union of Radio Science, Beijing, China, Aug. 16–23, 2014, Commission E, Paper E05.2.